Vibrational Spectra and Structures of Long-Chain Streptocyanine Dyes: Effects of Electron−Vibration Interactions and Vibrational Polarizabilities

Kazuhiko Furuya

Ashigara Research Laboratories, Fuji Photo Film Co. Ltd., 210 Nakanuma, Minami Ashigara, Kanagawa 250-0193, Japan

Hajime Torii*

Department of Chemistry, School of Science, The University of Tokyo, Bunkyo-ku, Tokyo 113-0033, Japan

Yukio Furukawa

Department of Chemistry, School of Science and Engineering, Waseda University, Shinjuku-ku, Tokyo 169-8555, Japan

Mitsuo Tasumi*

Department of Chemistry, Faculty of Science, Saitama University, Urawa, Saitama 338-8570, Japan

Received: June 27, 2000; In Final Form: September 14, 2000

The structural and vibrational properties of streptocyanine dyes, expressed as $[(CH_3)_2N(CH)_xN(CH_3)_2]^+ClO_4^-$ (called SC*x* in this paper) with $x = 2n + 1$ ($n = 0-10$), are examined by measuring the infrared (IR) and Raman spectra in solution and in the polycrystalline state (for $x = 1, 3, 7, 9$) and by carrying out density functional calculations at the BHandHLYP/6-31G* level. It is shown that the strong IR bands observed and calculated in the 1800−800 cm^{-1} region arise from the normal modes containing large contributions from the vibrations along the bond-alternation coordinate of the conjugated chains. As the conjugated chain becomes longer, the strongest IR band shifts toward the lower-wavenumber side, inducing noticeable changes in the spectral pattern, and the total IR intensity increases significantly. The shifts to lower wavenumbers and the changes in the spectral pattern are explained by the decrease in the intrinsic wavenumber of the bond-alternation mode. A two-state model Hamiltonian, which involves electron−vibration interaction of the bond-alternation mode, reasonably explains the IR intensity enhancement. In the Raman spectra of SC7 and SC9, a few strong bands appear in solution which are not seen in the polycrystalline state. These Raman bands are considered to arise from the same vibrational modes as the strong IR bands, as in the case of similar Raman bands observed previously for SC5 in solution. The relative Raman intensities of the bands are, however, larger in the spectra of SC7 and SC9. These results provide strong evidence for the validity of the mechanism proposed previously that the electron−vibration interaction in the conjugated chain and the intermolecular interaction with the perchlorate ions (existing at various positions near the conjugated chain in solution) give rise to the strong Raman intensities of these bands. It is also suggested that the appearance of these bands is a good signature of the large vibrational contributions to the polarizability tensors in this type of conjugated molecules. The diagonal and off-diagonal force constants of the CC stretches in the conjugated chains are analyzed. It is shown that the conjugated chains of streptocyanine dyes are more strongly correlated than those of neutral polyene chains.

1. Introduction

Cyanine dyes with conjugated methine chains are widely used as spectral sensitizers in the silver halide photographic system.[1−3] This is because the photosensitive region of silver halides may be altered by changing the chain lengths of the dyes and because the electronic absorption spectra of the dyes become very sharp as they form J-aggregates on the surface of silver halide grains. It is expected that the efficiency of cyanine dyes as spectral sensitizers may be improved by controlling the adsorption patterns of the dyes on silver halide grains. As a basis for analyzing the adsorption patterns of the cyanine dyes at the molecular level by vibrational spectroscopy, it is important to examine the vibrational spectra of the dyes themselves.[4−9]

Molecules with conjugated methine chains (including push−pull polyenes) have also been studied as materials exhibiting large nonlinear optical response.[10−22] It is suggested that the signs and magnitudes of the hyperpolarizabilities may be changed by controlling the bond alternation of the conjugated chains, which varies with the strengths of electron donors and acceptors on the chain ends (in push−pull polyenes) and/or with the intermolecular interactions with solvents.[13−21] It has been recognized that the vibrational contribution to the hyperpolar-

* To whom correspondence should be addressed. For H. Torii: fax, +81-3-3818-4621; e-mail, torii@chem.s.u-tokyo.ac.jp. For M. Tasumi: fax, +81-48-858-3379; e-mail, tasumi@chem.saitama-u.ac.jp.

10.1021/jp002308i CCC: $19.00 © 2000 American Chemical Society
Published on Web 11/04/2000

izabilities is comparable to (or sometimes larger than) the electronic one in this series of molecules.[19−22] Since dipole derivatives and polarizability derivatives with respect to vibrational coordinates determine the vibrational contribution,[23,24] it is important to examine the properties of these derivatives in detail. Studies on these derivatives are also important to gain deep insight into the features observed in the infrared (IR) and Raman spectra, because they determine the IR and Raman intensities of normal modes as well.

In our previous study,[9] the IR and Raman spectra of a pentamethine streptocyanine dye [(5-dimethylaminopenta-2,4-dienylidene)ammonium perchlorate, alias SC5] have been observed in dimethyl sulfoxide (DMSO) solution and in the polycrystalline state, and vibrational analysis has been carried out by comparing the observed spectra with those calculated by the density functional method. The features observed in the IR and Raman spectra have been shown to be well-reproduced by the calculations, indicating that the vibrational force field, dipole derivatives, and polarizability derivatives obtained from the calculations are sufficiently reliable. Some interesting characteristics have been clarified from the vibrational analysis. (1) Two strong IR bands observed at 1570 and 1206 cm^{-1} arise from the delocalized b_1 modes along the bond-alternation coordinate (mixed with the CH bends), in which the CC and NC bonds in the conjugated chain stretch and contract alternately, and the strong IR intensities are explained by the large charge fluxes induced by these modes due to the strong electron−vibration interaction. (2) The dipole derivatives of the CC and NC stretches of the conjugated chain are so large that the IR intensities of many normal modes are dominated by the contribution from the CC and NC stretches, even for some modes characterized as the methyl deformation or CH in-plane bending in terms of potential energy distribution. (3) The off-diagonal force constants for the CC and NC stretches in the conjugated chain are large in magnitude and decrease slowly as the relevant bonds become distant, as compared with the case of neutral polyene chains. It has been concluded from these results that the conjugated chain of SC5 is a more strongly correlated system than neutral polyene chains. To find out how general these findings are for streptocyanine dyes and how they depend on the chain length, it is necessary to carry out similar vibrational analyses for streptocyanine dyes with various chain lengths. Such analyses are crucial to correlate the observed spectral features to the structural and vibrational characteristics of the dyes, as well as to understand the mechanism giving rise to the spectral features.

We have also found in ref 9 that Raman bands with medium intensities appear at 1574 and 1207 cm^{-1} in solution which are not seen in the polycrystalline state. It is considered from the comparison of the observed and calculated vibrational wavenumbers that these Raman bands arise from the same vibrational modes as the strong IR bands observed at 1570 and 1206 cm^{-1}, in which the conjugated chain of SC5 vibrates along the bond-alternation coordinate. From the analysis employing a two-state model Hamiltonian,[21,25] it has been suggested that these modes appear in the Raman spectrum in solution because of the electron−vibration interaction in the conjugated chain and the intermolecular interaction with the perchlorate ions existing at various positions near the conjugated chain in solution.[21] As shown in eq 13 of ref 21, the polarizability derivative induced by this mechanism is approximately proportional to $(\mu_D/t)^2$, where μ_D is the electronic transition dipole moment and t is one-half the electronic excitation energy. It is therefore expected that stronger Raman bands of similar character may be observed for longer cyanine dyes in solution. Observation of such bands will provide strong evidence for the validity of the mechanism of generating Raman intensities proposed in ref 21.

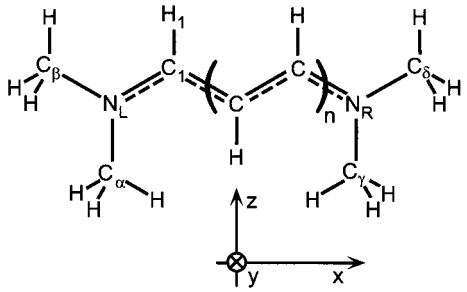

Figure 1. Coordinate axes and the numbering of atoms for the organic portion of SC(2*n*+1).

In the present study, we observe the IR and Raman spectra of streptocyanine dyes with one to nine methine groups, expressed as $[(CH_3)_2N(CH)_xN(CH_3)_2]^+ClO_4^-$ with $x = 1$, 3, 7, and 9 (Figure 1, denoted by SC*x* hereafter), and compare the observed spectra with those calculated by the density functional method, complementing our previous study[9] on a pentamethine streptocyanine dye ($x = 5$). Calculations are also carried out for streptocyanine dyes with longer conjugated chains ($x = 2n + 1$ with $n = 5-10$). The chain length dependence of the vibrational properties is examined in detail.

2. Experimental and Computational Procedures

IR spectra were measured in DMSO solution and in KBr disk on Fourier transform IR spectrophotometers (Nicolet 5DX and Digilab FTS-40) at 4 cm^{-1} resolution. Raman spectra were measured on a Fourier transform Raman spectrophotometer (Bruker RFS-100) with 1064 nm excitation at 2 cm^{-1} resolution, both in DMSO-d_6 solution and in the polycrystalline (powder) state, except for the Raman spectrum of SC9 in the polycrystalline state, which was measured on a JEOL JIR-5500 Fourier transform Raman spectrophotometer with 1320 nm excitation at 4 cm^{-1} resolution.

Density functional (DF) calculations were performed by using the BHandHLYP (Becke's half-and-half hybrid method[26] with the Lee−Yang−Parr correlation[27,28]) functional in combination with the 6-31G* basis set. The Gaussian 92/DFT and Gaussian 94 programs[29,30] were used on Kubota TITAN-3020 and Silicon Graphics Power Onyx workstations. Part of the calculations were carried out on IBM SP2 computers at the Computer Center of the Institute for Molecular Science. The perchlorate ion was not included in the calculations. The cationic (organic) portion of SC*x* is called the SC*x* organic portion (abbreviated as SC*x*OP) hereafter. Numerical integration of functionals were performed by using the "fine" integration grid in both the Gaussian 92/DFT and Gaussian 94 programs.

Based on the vibrational force fields obtained from the DF calculations, vibrational analyses were carried out with the programs written by one of the authors (H.T.) on M880 and S-3800 computers at the Computer Center of the University of Tokyo.

3. Results and Discussion

A. Observed and Calculated Spectra and Characterization of Normal Modes. The IR spectra of SC1, SC3, SC7, and SC9 observed in DMSO solution are shown in Figures 2a,c and 3a,c, respectively. Solvent bands are subtracted in these spectra. The strongest IR band is observed at 1701 cm^{-1} for SC1, 1626 cm^{-1} for SC3, 1570 cm^{-1} for SC5,[9] 1534 cm^{-1} for SC7, and 1507

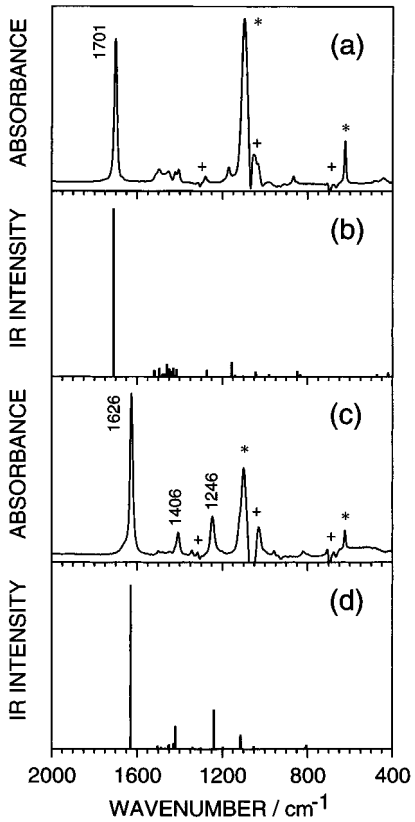

Figure 2. IR spectra of SC1 (a) observed in DMSO solution and (b) calculated at the BHandHLYP/6-31G* level and IR spectra of SC3 (c) observed in DMSO solution and (d) calculated at the BHandHLYP/6-31G* level. The solvent bands remaining after subtraction are marked with pluses (+). The bands originating from the perchlorate ion are marked with asterisks (*).

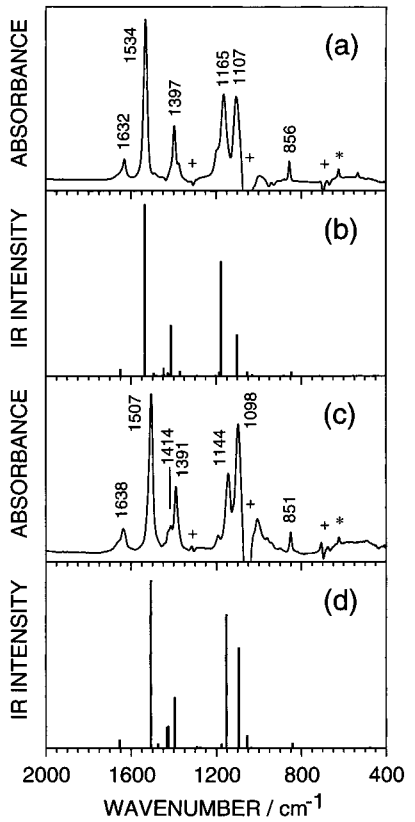

Figure 3. IR spectra of SC7 (a) observed in DMSO solution and (b) calculated at the BHandHLYP/6-31G* level and IR spectra of SC9 (c) observed in DMSO solution and (d) calculated at the BHandHLYP/6-31G* level. See also the caption for Figure 2.

cm^{-1} for SC9, indicating a gradual decrease in wavenumber as the chain length increases. The IR intensity of this band, as compared with those of the perchlorate bands marked with asterisks, increases significantly as the conjugated chain becomes longer. It is also noticed that the IR bands in the 1170−1090 cm^{-1} region become stronger as the chain length increases.

The IR spectra of SC*x* ($x = 1, 3, 7, 9$) observed in KBr disk are shown in Figure 4. All the IR bands observed in KBr disk are significantly broader than those observed in solution, and the bands in the 1200−800 cm^{-1} region are congested and overlap significantly with perchlorate bands, as in the case of the IR spectrum of SC5.[9] However, the decrease in the wavenumber of the strong IR band in the 1800−1400 cm^{-1} region is clearly seen also in this figure.

The IR spectra of SC*x*OP ($x = 1, 3, 7, 9$) calculated at the BHandHLYP/6-31G* level are shown in Figures 2b,d and 3b,d. It is seen that the calculated vibrational wavenumbers (scaled uniformly by 0.9326, which is obtained by least-squares fitting) and relative IR intensities are in good agreement with the experimental results. It is especially noted that good agreement is obtained for the wavenumber of the strongly IR-active mode in the 1720−1500 cm^{-1} region, which is sensitive to the computational level as shown in Figure 5 of our previous study[9] for SC5OP. This result supports the validity of using the BHandHLYP functional for calculating the vibrational spectra of this series of molecules. It is also noticed that the increase in the relative IR intensities of the modes in the 1170−1090 cm^{-1} region for longer chains is well-reproduced by the calculations. The vibrational force fields and the dipole derivatives obtained from the calculations are considered to be sufficiently reliable. The chain-length dependence of the calculated total IR intensities will be discussed in section 3B.

The vibrational patterns of some strongly IR-active modes of SC7OP and SC9OP are shown in Figures 5 and 6, respectively. The normal modes are numbered in the same way as those of SC5OP.[9] It is clearly seen that the CC and NC bonds in the conjugated chains stretch and contract alternately in ν_{38} and ν_{49} of SC7OP and in ν_{44} and ν_{56} of SC9OP, which are strongly IR-active. These modes are therefore described as delocalized vibrations along the bond-alternation coordinate of the conjugated chains (mixed with the CH bends), and their strong IR intensities are explained by large charge fluxes induced in the chains.[9,25,31−33] For the other four modes shown in Figures 5 and 6, however, the contributions of the vibrations along the bond-alternation coordinate are smaller.

To examine the origin of the IR intensities in more detail for the modes shown in Figures 5 and 6, the values of $\partial\mu_x/\partial S_j \times \partial S_j/\partial Q_m$ and the potential energy distribution (PED) are calculated and shown in Tables 1 and 2, where $\partial\mu_x/\partial S_j$ is the x component (along the chain axis) of the dipole derivative with respect to molecular symmetry coordinate S_j, and Q_m is the mth normal coordinate. The molecular symmetry coordinates are defined and numbered in the same way as those of SC5OP,[9] and the brief description of the coordinates involved is indicated in the tables. As explained in ref 9, $\partial\mu_x/\partial S_j \times \partial S_j/\partial Q_m$ indicates the contribution of each symmetry coordinate to the IR intensity of the mth normal mode, which is proportional to $|\partial\boldsymbol{\mu}/\partial Q_m|^2$.

For ν_{38} and ν_{49} of SC7OP and for ν_{44} and ν_{56} of SC9OP, it is seen that the contribution of the CC and NC stretches of the conjugated chains ($S_{30}-S_{34}$ for SC7OP and $S_{34}-S_{38}$ for SC9OP) is predominant in terms of both $\partial\mu_x/\partial S_j \times \partial S_j/\partial Q_m$ and PED. This result supports the view described above that the IR

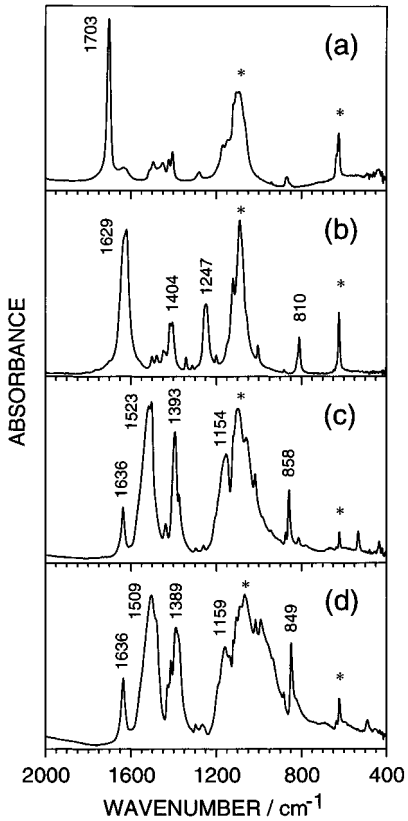

Figure 4. IR spectra of (a) SC1, (b) SC3, (c) SC7, and (d) SC9 observed in KBr disk. See also the caption for Figure 2. The center of half-height is indicated for the strongest IR band (1703 cm^{-1} for SC1, 1629 cm^{-1} for SC3, 1523 cm^{-1} for SC7, and 1509 cm^{-1} for SC9).

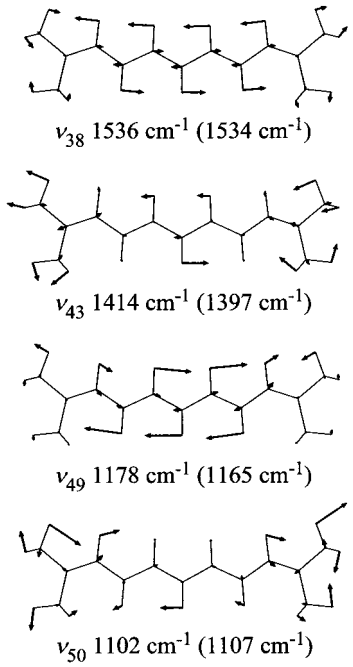

Figure 5. Vibrational patterns of the modes of SC7OP inducing strong IR intensities. The mode numbers and the calculated (observed) wavenumbers are indicated.

intensities of these modes derive from large charge fluxes in the conjugated chains. For most of the other modes shown in the tables, the contributions of the methyl bends and rocks are large in terms of PED. However, for these modes also the contributions of the CC and NC stretches of the conjugated chains are significant in terms of $\partial\mu_x/\partial S_j \times \partial S_j/\partial Q_m$, indicating

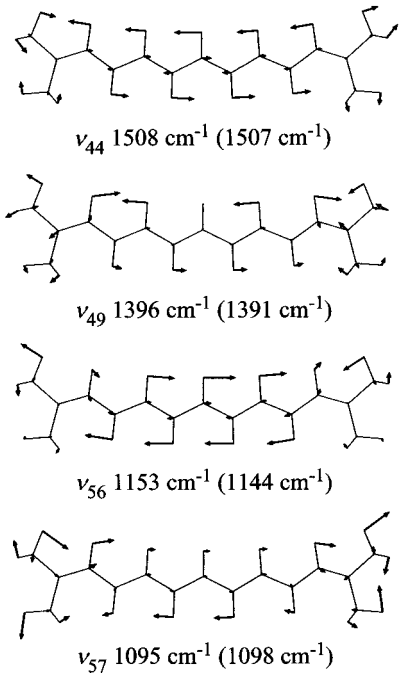

Figure 6. Vibrational patterns of the modes of SC9OP inducing strong IR intensities. The mode numbers and the calculated (observed) wavenumbers are indicated.

their large contributions to the IR intensities of these modes. As suggested in our previous study on SC5OP,[9] PED is not necessarily a good indicator of the origin of IR intensity.

The Raman spectra of SCx (x = 1, 3, 7, 9) observed in DMSO-d_6 solution are shown in Figure 7. For SC1 (Figure 7a), a single strong Raman band is observed at 1424 cm^{-1}, which mainly arises from the symmetric bending of the methyl groups at the β and δ positions (see Figure 1). In the Raman spectrum of SC3 (Figure 7b), a few bands are observed with significant intensities. The strongest band is observed at 1656 cm^{-1}, and arises from a delocalized vibration of the conjugated chain mixed with the CH bends. The character of this mode is similar to that of ν_8 (at 1658 cm^{-1}) of SC5.[9] The above spectral features are also seen in the Raman spectra observed in the polycrystalline state, which are shown in Figure 8a,b.

In the case of SC7, however, the spectral pattern observed in DMSO-d_6 solution is different from that observed in the polycrystalline state. As shown in Figure 7c, Raman bands with significant intensities are observed at 1645, 1567, 1536, 1406, 1304, 1192, 1165, and 1123 cm^{-1} in solution. Among these, the bands at 1536 and 1165 cm^{-1} are not observed in the polycrystalline state shown in Figure 8c. These two Raman bands are considered to arise from the same vibrational modes as the strong IR bands observed at 1534 and 1165 cm^{-1} (Figure 3a), characterized as the vibrations along the bond-alternation coordinate of the conjugated chain (mixed with the CH bends). In the case of SC9, the Raman bands at 1634, 1413, 1299, and 1124 cm^{-1} are observed both in solution and in the polycrystalline state, but the bands at 1512, 1147, and 1101 cm^{-1} are observed only in solution. The latter three bands are also considered to arise from the same vibrational modes as the strong IR bands, which are observed for this molecule at 1507, 1144, and 1098 cm^{-1} (Figure 3c), to which the contributions of the vibration along the bond-alternation coordinate are significant as shown in Table 2. While the Raman bands of the same character have only medium intensities in the case of SC5,[9] the 1536 cm^{-1} band of SC7 and the 1512 cm^{-1} band of SC9 are the strongest in their Raman spectra, in accord with the

TABLE 1: $\partial\mu_x/\partial S_j \times \partial S_j/\partial Q_m$ and Potential Energy Distribution of the Strongly IR-Active b_1 Modes of the Organic Portion of SC7

	observed	calculated					
mode	wavenumber (cm^{-1})	wavenumber (cm^{-1})	IR intensity (km mol^{-1})		coordinate[a]	$\partial\mu_x/\partial S_j \times \partial S_j/\partial Q_m$ (D $Å^{-1}$ $amu^{-1/2}$)	PED (%)
ν_{38}	1534	1536	6480	S_{30}	(NC_1 str)	2.273	6.7
				S_{31}	(C_1C_2 str)	3.131	15.1
				S_{32}	(C_2C_3 str)	3.989	20.7
				S_{33}	(C_3C_4 str)	4.069	20.8
				S_{46}	(C_1H_1 bend)	−0.249	14.7
				S_{47}	(C_2H_2 bend)	0.039	14.2
				S_{48}	(C_3H_3 bend)	−0.132	18.1
				S_{55}	(Me_β sym bend)	−0.461	9.2
				total		12.384	
ν_{43}	1397	1414	1945	S_{30}	(NC_1 str)	3.908	23.5
				S_{32}	(C_2C_3 str)	−0.414	0.3
				S_{33}	(C_3C_4 str)	1.935	5.5
				S_{34}	(NC_α str)	0.586	6.8
				S_{35}	(NC_β str)	0.588	6.9
				S_{52}	(Me_α sym bend)	0.283	23.2
				S_{55}	(Me_β sym bend)	0.732	27.5
				total		6.784	
ν_{49}	1165	1178	4339	S_{30}	(NC_1 str)	0.839	1.6
				S_{31}	(C_1C_2 str)	3.262	27.8
				S_{32}	(C_2C_3 str)	2.390	12.7
				S_{33}	(C_3C_4 str)	3.428	25.1
				S_{47}	(C_2H_2 bend)	−0.026	10.4
				total		10.134	
ν_{50}	1107	1102	1581	S_{30}	(NC_1 str)	2.740	19.0
				S_{32}	(C_2C_3 str)	1.469	5.5
				S_{33}	(C_3C_4 str)	1.017	2.5
				S_{35}	(NC_β str)	0.533	9.3
				S_{54}	(Me_α ip rock)	−0.041	9.8
				S_{57}	(Me_β ip rock)	0.731	39.6
				total		6.117	

[a] As in Table 3 of ref 9, each coordinate is defined as a linear combination of symmetry-related local coordinates. For example, S_{30} is defined as $[\sigma(N_LC_1) - \sigma(N_RC_7)]/\sqrt{2}$.

expectation for the intensity enhancement described in section 1. These results support the conclusion obtained in ref 21, from the analysis based on a two-state model, that the electron−vibration interaction in the conjugated chain and the intermolecular interaction with the perchlorate ions existing at various positions near the conjugated chain give rise to significant Raman intensities in solution for the modes with large contribution of the vibration along the bond-alternation coordinate, while in the crystalline state the perchlorate ions are expected[34] to be located at symmetric positions and do not give rise to such large Raman intensities. In other words, the conjugated chains are deformed in solution along the bond-alternation coordinate because of the large vibrational contributions to the polarizability tensors and the electrostatic intermolecular interactions. A similar 'symmetry breaking' effect has recently been observed in the resonance Raman spectra of I_3^- in solution.[35,36] According to the two-state model (eq 12 of ref 21), the IR intensities do not change significantly by such a symmetry-breaking effect, in accord with the spectral features observed in Figures 3 and 4 for SC7 and SC9. The symmetry-breaking effect induced by intermolecular interactions treated above is different from 'spontaneous' symmetry breaking treated in ref 37, while electron−vibration interactions are important in both cases. The role of electron−vibration interactions and electrostatic intermolecular interactions in generating spectral features deserves further studies.

B. Chain Length Dependence of the Wavenumber of the Bond-Alternation Mode and the Total IR Intensity. The IR spectra and the intrinsic vibrational wavenumber (ν_{BA}) of the bond-alternation mode (BAM) calculated for SC(2*n*+1)OP (*n* = 0−10) are shown in Figure 9. The intensity scale is different for each species. The bond-alternation coordinate S_{BA} is defined as

$$S_{BA} = [\sigma(N_LC_1) + \sum_{i=1}^{n} \{-\sigma(C_{2i-1}C_{2i}) + \sigma(C_{2i}C_{2i+1})\} - \sigma(C_{2n+1}N_R)] \times (2n+2)^{-1/2} \quad (1)$$

where σ(XY) denotes the stretching coordinate of the X−Y bond and the numbering of atoms is shown in Figure 1. The intrinsic vibrational wavenumber ν_{BA} is calculated as

$$\nu_{BA} = 1302.791 \times (f_{BA}g_{BA})^{1/2} \quad (2)$$

where f_{BA} is the diagonal force constant [scaled by $(0.9326)^2$] for S_{BA} and g_{BA} is the corresponding diagonal element of the **G** matrix.

In the IR spectrum of the shortest chain (*n* = 0), there is only a single strong IR band at 1710 cm^{-1}, and it is close to the intrinsic wavenumber of the BAM (1647 cm^{-1}). As the conjugated chain becomes longer (in the range of $n \leq 4$), the strongest IR band gradually moves toward the low-wavenumber side to 1508 cm^{-1} for *n* = 4, as described in section 3A, but the intrinsic wavenumber of the BAM moves to a greater extent (to 1340 cm^{-1} for *n* = 4) so that they get gradually separated from each other. At the same time, the IR intensities of the normal modes in the 1200−1000 cm^{-1} region become larger. At *n* = 5, normal modes with significant IR intensities exist in

TABLE 2: $\partial\mu_x/\partial S_j \times \partial S_j/\partial Q_m$ and Potential Energy Distribution of the Strongly IR-Active b_1 Modes of the Organic Portion of SC9

	observed	calculated					
mode	wavenumber (cm^{-1})	wavenumber (cm^{-1})	IR intensity (km mol^{-1})		coordinate[a]	$\partial\mu_x/\partial S_j \times \partial S_j/\partial Q_m$ (D $Å^{-1}$ $amu^{-1/2}$)	PED (%)
ν_{44}	1507	1508	8662	S_{34}	(NC_1 str)	2.133	4.2
				S_{35}	(C_1C_2 str)	2.554	7.8
				S_{36}	(C_2C_3 str)	3.148	9.4
				S_{37}	(C_3C_4 str)	3.646	13.3
				S_{38}	(C_4C_5 str)	4.529	18.2
				S_{53}	(C_1H_1 bend)	−0.245	11.5
				S_{55}	(C_3H_3 bend)	−0.106	10.7
				S_{56}	(C_4H_4 bend)	0.034	13.6
				S_{63}	(Me_β sym bend)	−0.744	15.7
				total		14.318	
ν_{49}	1391	1396	2652	S_{34}	(NC_1 str)	4.698	23.9
				S_{35}	(C_1C_2 str)	−0.737	0.8
				S_{36}	(C_2C_3 str)	1.067	1.3
				S_{37}	(C_3C_4 str)	1.613	3.0
				S_{39}	(NC_α str)	1.040	14.4
				S_{55}	(C_3H_3 bend)	−0.101	11.3
				S_{63}	(Me_β sym bend)	0.451	6.7
				S_{64}	(Me_β ip asym bend)	−0.220	10.1
				S_{65}	(Me_β ip rock)	−0.456	6.3
				total		7.923	
ν_{56}	1144	1153	6911	S_{35}	(C_1C_2 str)	3.195	20.8
				S_{36}	(C_2C_3 str)	2.879	13.4
				S_{37}	(C_3C_4 str)	2.928	14.7
				S_{38}	(C_4C_5 str)	3.675	20.5
				S_{65}	(Me_β ip rock)	−0.559	14.0
				total		12.788	
ν_{57}	1098	1095	5226	S_{34}	(NC_1 str)	3.520	21.8
				S_{35}	(C_1C_2 str)	0.482	0.5
				S_{36}	(C_2C_3 str)	1.930	6.7
				S_{37}	(C_3C_4 str)	2.214	9.3
				S_{38}	(C_4C_5 str)	1.753	5.2
				S_{40}	(NC_β str)	0.627	10.4
				S_{62}	(Me_α ip rock)	−0.043	12.9
				S_{65}	(Me_β ip rock)	0.751	27.9
				total		11.121	

[a] See corresponding footnote for Table 1.

the 1500−1400 and 1150−1050 cm^{-1} regions, and the intrinsic wavenumber of the BAM (1284 cm^{-1}) lies halfway between the two regions. The strongest IR band is now seen at 1080 cm^{-1}. As the chain length further increases ($n = 6-9$), this strongest IR band moves gradually toward the low-wavenumber side to 925 cm^{-1} for $n = 9$, but the intrinsic wavenumber of the BAM moves to a greater extent (to 1072 cm^{-1} for $n = 9$) so that they gradually approach each other. The relative weight of the strongest IR band is so large at $n = 7-9$ that this band predominates in the IR spectra. At $n = 10$, it is seen that the strongest IR-active mode is mixed with another mode so that there are two strong IR bands at 882 and 837 cm^{-1}.

These results suggest that the vibration along S_{BA} is the main origin of the IR intensities and the mixing of the BAM with other vibrations determines the main features of the IR spectra. As the conjugated chain becomes longer, the intrinsic wavenumber of the BAM decreases and strong IR bands appear in a lower-wavenumber region. This conclusion is consistent with that obtained in section 3A from the comparison of the observed and calculated IR spectra and the detailed vibrational analyses carried out for SC(2n+1)OP with $n = 0-4$. It is also consistent with previous theoretical studies[33,38,39] suggesting that variation in the force constant for S_{BA} (or equivalently the electron−vibration coupling parameter[38,39]) gives rise to the difference in the wavenumbers of the strong IR bands observed for doped and photoexcited polyacetylene chains.

The chain-length dependence of the total IR intensity is shown in Figure 10. An approximate quadratic dependence of the IR intensity on n is clearly seen. In other words, the relevant dipole derivative is approximately proportional to n. This result is reasonably explained by considering that the vibration along S_{BA} is mainly responsible for the IR intensities and by employing the two-state model Hamiltonian presented in our previous studies.[21,25] According to the formulation based on the model Hamiltonian, the dipole derivative with respect to S_{BA}, $\partial\mu/\partial S_{BA}$, is expressed as

$$\frac{\partial\mu}{\partial S_{BA}} \cong \frac{2k_{BA}S_0\mu_D}{E_{eg}} \tag{3}$$

where k_{BA} is the diagonal force constant for S_{BA}, S_0 is one-half the difference in the value of S_{BA} between the minima of the two diabatic potential energy curves supposed in the model Hamiltonian, and μ_D and E_{eg} are the transition dipole moment and the excitation energy, respectively, of the electronic transition between the two adiabatic states. k_{BA}, S_0, and E_{eg} are equal, respectively, to $2k$, Q_0, and $2t$ in the notation used in ref 21 and 25. k_{BA} is obtained from the calculations at the BHandHLYP/6-31G* level described above. S_0 is estimated to be $0.05 \times (2n + 2)^{1/2}$ [Å] in the same way as in refs 21 and 25. (However, in contrast to refs 21 and 25, the CN stretches are included in S_{BA} in the present study to maintain consistency

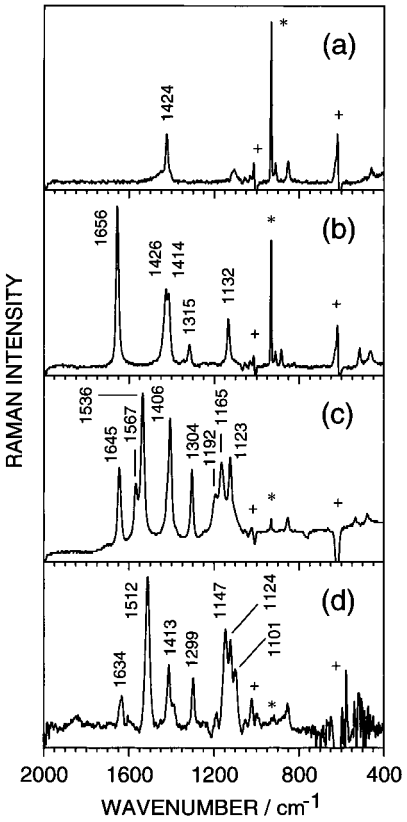

Figure 7. Raman spectra of (a) SC1, (b) SC3, (c) SC7, and (d) SC9 observed in DMSO-d_6 solution. See also the caption for Figure 2.

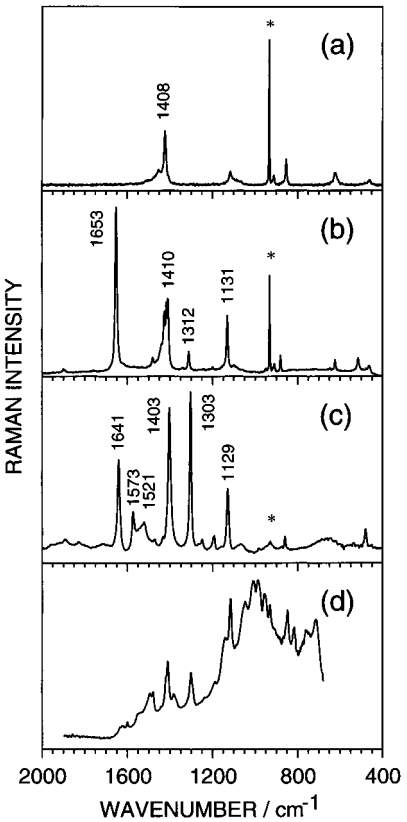

Figure 8. Raman spectra of (a) SC1, (b) SC3, (c) SC7, and (d) SC9 observed in the polycrystalline state. See also the caption for Figure 2.

with the analysis shown in Figure 9.) μ_D and E_{eg} may be obtained by carrying out ab initio molecular orbital (MO) calculations for the electronic excited state. In the present study,

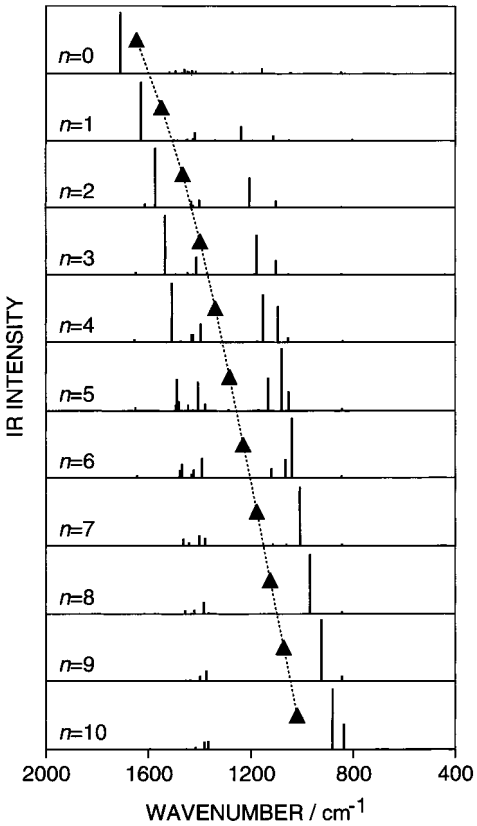

Figure 9. IR spectra (bars) and intrinsic vibrational wavenumbers of the bond-alternation mode (triangles connected with broken lines) calculated for SC(2n+1)OP (n = 0−10).

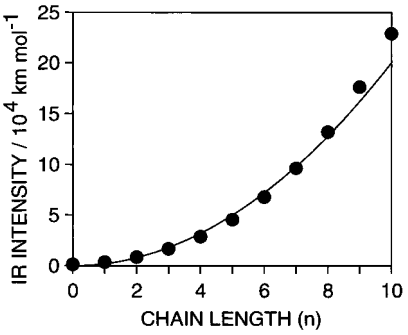

Figure 10. Chain-length dependence of the calculated total IR intensities of SC(2n+1)OP (filled circles). The solid line (drawn as a guide to the eye) indicates a quadratic dependence on the chain length (n).

calculations at the CIS (configuration interaction singles)[40] level with the 6-31G* basis set have been performed to estimate the values of μ_D and E_{eg} for SC(2n+1)OP with n = 2−10.

The values of $\partial\mu/\partial S_{BA}$ estimated by using eq 3 and the parameters involved in this equation are shown in the second through sixth columns of Table 3. It is clearly seen that an approximate linear dependence of $\partial\mu/\partial S_{BA}$ on n is obtained, especially in the range of $n \leq 8$. Compared with the values of $\partial\mu/\partial S_{BA}$ directly obtained from the calculations at the BHandHLYP/6-31G* level, the values estimated by eq 3 are slightly smaller. However, scaling of the latter values by 1.33 (the seventh column) results in good agreement in the range of $n \leq 8$. The values of $\partial\mu/\partial S_{BA}$ estimated by eq 3 tend to saturate for SC(2n+1)OP with $n \geq 9$, but those directly calculated at the BHandHLYP/6-31G* level do not. This discrepancy, as well as the difference in the absolute values of $\partial\mu/\partial S_{BA}$ obtained by the two methods, may arise from the lack of sufficient reliability

TABLE 3: dμ/dS for the Bond-Alternation Coordinate (S_{BA}) of the Organic Portion of SC(2n+1) Derived from a Theoretical Model and from DF Calculations and the Parameters Used in the Model

					dμ/dS_{BA} (D Å^{-1})		
n	μ_D (D)	E_{eg} (eV)	k_{BA} (mdyn Å^{-1})	S_0 (Å)	model	model, scaled	direct calcd
2	10.3	4.50	5.28	0.122	18.5	24.6	26.7
3	12.7	3.78	4.71	0.141	28.0	37.3	38.0
4	14.9	3.29	4.27	0.158	38.2	50.9	50.3
5	17.0	2.94	3.89	0.173	48.6	64.8	63.6
6	18.9	2.67	3.55	0.187	58.6	78.1	77.8
7	20.6	2.46	3.24	0.200	67.7	90.3	92.9
8	22.2	2.29	2.94	0.212	75.6	100.8	108.9
9	23.6	2.15	2.67	0.224	81.7	109.0	125.9
10	25.0	2.05	2.41	0.235	86.0	114.7	143.5

in the values of μ_D and/or E_{eg} calculated at the CIS/6-31G* level (especially overestimation in the values of E_{eg} at this theoretical level), from the rough estimation of the values of S_0, from some factors not involved in the model Hamiltonian, and/or from systematic overestimation of $\partial\mu/\partial S_{BA}$ at the BHandHLYP/6-31G* level.

C. Vibrational Force Constants. The calculated diagonal force constants for the CC stretches of SC(2n+1)OP (n = 1−10) are plotted against the CC bond lengths in Figure 11. An approximate linear relationship between the two quantities is clearly seen. In other words, the vibrational force field of the conjugated chain in each species is strongly related to its structure.

As shown in Figure 7 of ref 41, a similar linear relationship has been obtained for the C═C and C−C stretches of neutral polyene chains, although the gradients of the lines obtained from linear regression are different between the C═C and C−C stretches. The diagonal force constants of the C═C and C−C stretches are distributed in the 7−10 and 4.5−5.5 mdyn Å^{-1} regions, respectively, and the linear regression lines in these two regions intersect around the point with the bond length of 1.4 Å and the force constant of 6 mdyn Å^{-1}, which falls in the region shown in Figure 11 of the present study. The points plotted in Figure 11 therefore interpolate the regions of typical C═C and C−C bonds.

The calculated off-diagonal (coupling) force constants for the CC stretches of SC21OP are plotted against the separation of the relevant CC bonds (m for the jth and (j+m)th CC bonds) in Figure 12a. The force constant is positive if m is odd and negative if m is even, and the magnitude decreases gradually as m increases. The same behavior is also seen for the coupling force constants of the C═C and C−C stretches of neutral polyene chains,[41] where the force constant is negative between two C═C bonds and between two C−C bonds and positive between C═C and C−C bonds, and the magnitude decreases as the relevant bonds become distant.

However, the magnitude of the coupling force constant varies more slowly with m in streptocyanine dyes. The magnitude of the coupling force constant involving the first CC bond is shown as a semilog plot in Figure 12b, separately for the positive and negative force constants. The gradient of this plot is about −0.04 in the range of $m \geq 5$. By contrast, the gradient of a similar plot for neutral polyene chains is about −0.2, as indicated in ref 41 as the exponent in the empirical expressions derived for fitting the calculated force constants.[42] It is therefore concluded that the conjugated chains in streptocyanine dyes are more strongly correlated than those in neutral polyene chains.

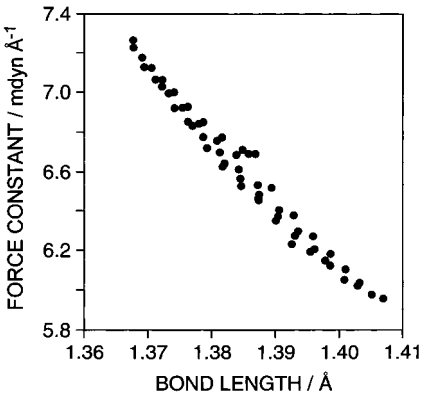

Figure 11. Relation between the CC bond lengths and the relevant diagonal force constants in the conjugate chains of SC(2n+1)OP (n = 1−10).

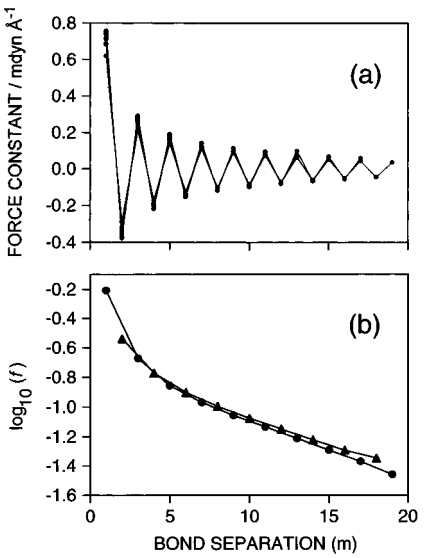

Figure 12. (a) Off-diagonal force constants between the CC stretches in the conjugated chains of SC21OP as a function of the separation (m) between the relevant CC bonds. (b) Semi-log plot of the magnitudes of the off-diagonal force constants involving the first CC bond in the conjugated chains of SC21OP, drawn separately for positive (circles) and negative (triangles) force constants.

4. Concluding Remarks

In the present study, the structural and vibrational properties of streptocyanine dyes are examined both experimentally and theoretically, with special emphasis on their chain-length dependence. It is shown that the main features in the IR spectra are determined by the normal modes with large contributions from the vibration along S_{BA}, because large dipole derivatives are induced in the conjugated chains by these modes owing to the strong electron−vibration interactions. The total IR intensity increases quadratically as the chain length increases. The same modes also appear in the Raman spectra in solution (for $n \geq 2$) because of the symmetry breaking induced in the conjugated chains by the electron−vibration interactions and the electrostatic intermolecular interactions. This spectral feature also becomes more prominent as the chain length increases. These results are reasonably explained by the two-state model Hamiltonian employed in our previous studies,[21,25] demonstrating the validity and usefulness of this model Hamiltonian. It is hoped that the knowledge obtained in the present study on the mechanism giving rise to the spectral features of streptocyanine dyes is useful in gaining deep insight into the correlation among the structural, electronic, and vibrational properties of molecules

with conjugated π electron systems in general and in improving the efficiency of these molecules in various practical applications.

Acknowledgment. The authors thank Mr. Satoshi Ando and Dr. Akira Sakamoto for their help in measuring the Raman spectrum of SC9 in the polycrystalline state with 1320 nm excitation.

References and Notes

(1) West, W.; Gilman, P. B., Jr. In *The Theory of the Photographic Process*, 4th ed.; James, T. H., Ed.; Macmillan: New York, 1977; Chapter 10.

(2) Herz, A. H. In *The Theory of the Photographic Process*, 4th ed.; James, T. H., Ed.; Macmillan: New York, 1977; Chapter 9.

(3) Herz, A.; Danner, R.; Janusonis, G. *Adsorption from Aqueous Solution, Advances in Chemistry Series 79*; American Chemical Society: Washington, DC, 1968; p 173.

(4) Sano, N.; Shimizu, M.; Tanaka, J.; Tasumi, M. *J. Raman Spectrosc.* **1988**, *19*, 395.

(5) Brandt, E. S. *Appl. Spectrosc.* **1988**, *42*, 882.

(6) Wang, J.; Zhang, P.; He, T.; Xin, H.; Liu, F.-C. *J. Phys. Chem.* **1988**, *92*, 1942.

(7) He, T.-J.; Lin, C.-S.; Xin, H.-W.; Liu, F.-C. *J. Photogr. Sci.* **1989**, *37*, 2.

(8) Iwata, K.; Weaver, W. L.; Gustafson, T. L. *J. Phys. Chem.* **1992**, *96*, 10219.

(9) Furuya, K.; Inagaki, Y.; Torii, H.; Furukawa, Y.; Tasumi, M. *J. Phys. Chem. A* **1998**, *102*, 8413.

(10) Marder, S. R.; Beratan, D. N.; Cheng, L.-T. *Science* **1991**, *252*, 103.

(11) Cheng, L.-T.; Tam, W.; Stevenson, S. H.; Meredith, G. R.; Rikken, G.; Marder, S. R. *J. Phys. Chem.* **1991**, *95*, 10631.

(12) Marder, S. R.; Perry, J. W.; Bourhill, G.; Gorman, C. B.; Tiemann, B. G.; Mansour, K. *Science* **1993**, *261*, 186.

(13) Marder, S. R.; Perry, J. W.; Tiemann, B. G.; Gorman, C. B.; Gilmour, S.; Biddle, S. L.; Bourhill, G. *J. Am. Chem. Soc.* **1993**, *115*, 2524.

(14) Gorman, C. B.; Marder, S. R. *Proc. Natl. Acad. Sci. U.S.A.* **1993**, *90*, 11297.

(15) Marder, S. R.; Gorman, C. B.; Meyers, F.; Perry, J. W.; Bourhill, G.; Brédas, J.-L.; Pierce, B. M. *Science* **1994**, *265*, 632.

(16) Lu, D.; Chen, G.; Perry, J. W.; Goddard, W. A., III. *J. Am. Chem. Soc.* **1994**, *116*, 10679.

(17) Chen, G.; Lu, D.; Goddard, W. A., III. *J. Chem. Phys.* **1994**, *101*, 5860.

(18) Chen, G.; Mukamel, S. *J. Am. Chem. Soc.* **1995**, *117*, 4945; *J. Chem. Phys.* **1995**, *103*, 9355.

(19) Castiglioni, C.; Del Zoppo, M.; Zerbi, G. *Phys. Rev. B* **1996**, *53*, 13319.

(20) Cho, M. *J. Phys. Chem. A* **1998**, *102*, 703.

(21) Torii, H.; Furuya, K.; Tasumi, M. *J. Phys. Chem. A* **1998**, *102*, 8422.

(22) Bishop, D. M.; Champagne, B.; Kirtman, B. *J. Chem. Phys.* **1998**, *109*, 9987.

(23) Bishop, D. M. *Rev. Mod. Phys.* **1990**, *62*, 343.

(24) Bishop, D. M. *Adv. Chem. Phys.* **1998**, *104*, 1.

(25) Torii, H.; Tasumi, M. *J. Phys. Chem. B* **1997**, *101*, 466.

(26) Becke, A. D. *J. Chem. Phys.* **1993**, *98*, 1372.

(27) Lee, C.; Yang, W.; Parr, R. G. *Phys. Rev. B* **1988**, *37*, 785.

(28) Miehlich, B.; Savin, A.; Stoll, H.; Preuss, H. *Chem. Phys. Lett.* **1989**, *157*, 200.

(29) Frisch, M. J.; Trucks, G. W.; Schlegel, H. B.; Gill, P. M. W.; Johnson, B. G.; Wong, M. W.; Foresman, J. B.; Robb, M. A.; Head-Gordon, M.; Replogle, E. S.; Gomperts, R.; Andres, J. L.; Raghavachari, K.; Binkley, J. S.; Gonzalez, C.; Martin, R. L.; Fox, D. J.; Defrees, D. J.; Baker, J.; Stewart, J. J. P.; Pople, J. A. *Gaussian 92/DFT*; Gaussian, Inc.: Pittsburgh, PA, 1993.

(30) Frisch, M. J.; Trucks, G. W.; Schlegel, H. B.; Gill, P. M. W.; Johnson, B. G.; Robb, M. A.; Cheeseman, J. R.; Keith, T.; Petersson, G. A.; Montgomery, J. A.; Raghavachari, K.; Al-Laham, M. A.; Zakrzewski, V. G.; Ortiz, J. V.; Foresman, J. B.; Cioslowski, J.; Stefanov, B. B.; Nanayakkara, A.; Challacombe, M.; Peng, C. Y.; Ayala, P. Y.; Chen, W.; Wong, M. W.; Andres, J. L.; Replogle, E. S.; Gomperts, R.; Martin, R. L.; Fox, D. J.; Binkley, J. S.; Defrees, D. J.; Baker, J.; Stewart, J. J. P.; Head-Gordon, M.; Gonzalez, C.; Pople, J. A. *Gaussian 94*; Gaussian, Inc.: Pittsburgh, PA, 1995.

(31) Mele, E. J.; Rice, M. J. *Phys. Rev. Lett.* **1980**, *45*, 926.

(32) Horovitz, B. *Solid State Commun.* **1982**, *41*, 729.

(33) Gussoni, M.; Castiglioni, C.; Zerbi, G. *Spectroscopy of Advanced Materials;* Clark, R. J. H., Hester, R. E., Eds.; Wiley: New York, 1991; Advances in Spectroscopy, Vol. 19, p 251.

(34) In contrast to the case of SC5, there are no X-ray crystal analyses reported for SC7 and SC9 (perchlorate salt). However, by analogy with the results obtained for SC5, we expect that the perchlorate ions are located at symmetric positions also in the crystals of SC7 and SC9.

(35) Johnson, A. E.; Myers, A. B. *J. Phys. Chem.* **1996**, *100*, 7778.

(36) Sato, H.; Hirata, F.; Myers, A. B. *J. Phys. Chem. A* **1998**, *102*, 2065.

(37) Tolbert, L. M.; Zhao, X. *J. Am. Chem. Soc.* **1997**, *119*, 3253.

(38) Ehrenfreund, E.; Vardeny, Z.; Brafman, O.; Horovitz, B. *Phys. Rev. B* **1987**, *36*, 1535.

(39) Girlando, A.; Painelli, A.; Soos, Z. G. *J. Chem. Phys.* **1993**, *98*, 7459.

(40) Foresman, J. B.; Head-Gordon, M.; Pople, J. A.; Frisch, M. J. *J. Phys. Chem.* **1992**, *96*, 135.

(41) Hirata, S.; Torii, H.; Tasumi, M. *J. Chem. Phys.* **1995**, *103*, 8964.

(42) Note that the exponent obtained in ref 41 ($\cong -1$) is divided by 2 $\times$ 2.303 to match the definition of the ordinate and the abscissa in Figure 12b.